IGARSS 94
Special Issue

ANALYSIS OF SCATTERING MECHANISMS IN SAR IMAGERY OVER BOREAL FOREST: RESULTS FROM BOREAS'93

Mahta Moghaddam and Sasan Saatchi
Jet Propulsion Laboratory
MS 300-235
California Institute of Technology
4800 **Oak Grove Drive**
Pasadena, CA 91109

ABSTRACT

As part of the intensive field campaign (IFC) for the Boreal forest ecosystem-atmosphere research (B OREAS) project in August 1993, the NASA/JPL AIRSAR covered an area of about 100 km x 100 km near the Prince Albert National Park in Saskatchewan, Canada. At the same time, ground-truth measurements were made in several stands which have been selected as the primary study sites. This paper focuses on an area including Jack Pine stands in the Nipawin area near the park. Upon examining the AIRSAR data from stands of old and young Jack Pine (OJP and YJP), distinct signatures are observed for each of the forest types at various frequencies and polarizations. We use a forest scattering model in conjunction with the ground-truth measurements to explain such behavior. The forest model includes the major scattering mechanisms by taking the forest component interactions into account. The contribution from each of the scattering mechanisms to the total backscatter is calculated and their differences for OJP and YJP stands are evaluated. The results are used to discuss the effect of the physical properties of the forest components in each stand on radar backscatter. They are also used to show that it is not only the backscatter level but also the relative contribution from various scattering mechanisms that will help in quantitative interpretation of SAR data. This work is mainly intended as a precursor to our ongoing work which uses a mechanism-specific inversion technique to retrieve forest parameters from SAR data for these BOREAS sites.

1. INTRODUCTION

Over vegetated land surface, interpretation of radar backscatter data and development of techniques to either classify radar images or estimate vegetation parameters is dependent on understanding the scattering mechanisms that contribute to the backscatter signal level. For example, studies in the past few years have demonstrated that algorithms to estimate forest biomass benefit from the knowledge of the contribution of volume scattering, trunk-ground interaction, and other scattering mechanism terms at various polarizations or frequencies [1-4]. Although several methods have been developed to characterize the synthetic aperture radar (SAR) images in terms of dominant scattering mechanisms, the implementation of these methods over various forest stands and validation and generalization of the results are yet subject to investigation [5].

Here, we discuss the scattering properties of Jack pine forests, one of the dominant species in the boreal forest of Canada. Boreal forests cover a large area of the Northern hemisphere and have been the subject of many investigations in order to characterize their role in global biogeochemical cycles and climate studies. The area used for this work is part of a larger region used in the boreal ecosystem atmospheric study (BOREAS) project [6]. During several focused and intensive field campaigns in 1993 and 1994, SAR images were acquired over BOREAS study sites with the intention of mapping forest types and estimating parameters important in ecosystem modeling. The land cover types are characterized by few dominant species such as Aspen, Black Spruce, Jack pine, and bog and fen. The image we have chosen in this study covers an area with primarily two types of Jack pine stands: young Jack pine (YJP) at a regeneration stage with average age of 10-15 years, and old Jack pine (OJP) with average age of 65 years. These are located in the BOREAS Southern study area (SSA), near the Prince Albert National Park in Saskatchewan.

From SAR data, a strong distinction between YJ P and OJP backscatter has been observed, In the OJP stand the HH polarized backscatter at P-band (0.44 GHz) is much higher, up to 9 dB, than that of YJP stand, as well as VV backscatter in either stand. The OJP trees are taller (12-16 m) and have larger diameters, but are much more sparse than the YJP. The YJP trees. on the other hand, are shorter (2-4 m) and have denser and greener crown layer. The distinction in the backscatter over these two stands is consistent over the entire region. In order to understand this behavior and some other observations from SAR data, we have combined a classification technique, backscatter modeling, and the ground truth information acquired during the experiment. In this work, first some samples of SAR data at three frequencies (P-, L-, and C-band) and for all linear polarization combinations (HH, HV, and VV) are reported in Section 3. A forest backscatter model is then used, with the aid of ground truth measurements (Section 2), to identify the mechanisms contributing to the above effects at P-band. This is done in Section 4, where the results of the model

simulations, in addition to the classification of SAR images into scattering mechanisms without the ground truth data, are discussed. The effect of the incidence angle on the backscattering mechanisms are also considered. The results are then summarized with some concluding remarks in section 5.

2. THE EXPERIMENT

2.1. AIRSAR Data Collection

.4s part of the remote sensing activities in the August'93 campaign, the NASA/JPL airborne synthetic aperture radar (A IRSAR) acquired polarimetric C-, L-, and P-band backscattering data over the BOREAS sites both in the Southern and Northern study areas (SSA and NSA, respectively). These included diverse forest canopies such as Aspen, young and old Jack pines, and Black Spruce. Five locations in the south and four in the north were chosen as primary study areas, where flux towers were set up. In this work, we focus on the SAR data obtained on August 12 over an area in the SSA containing primarily Jack Pine trees. Figure 1 shows a map of the SSA with the AIRSAR flight lines. Trihedral corner reflectors were deployed in four locations throughout the area to be used as external devices for verifying the calibration of the data. The flight line of interest in this work is marked with an asterisk and corresponds to a heading of 57° with respect to true north. The radar is left-looking, and the size of the swath covered with a 20 MHz bandwidth is approximately 10km x 10km (1280 lines, 1024 pixels per line).

Among the locations covered in this line area young Jack Pine (YJP) stand, which is one of the areas selected as a flux tower site, and a nearby old Jack Pine (OJP) stand, which is not a flux tower site, but is similar to and within a few kilometers of the tower site OJP. In Figure 2 we have shown some photographs taken at typical locations in the YJP and OJP stands, respectively. These stands are quite uniform, and are thus excellent candidates for modeling studies. Furthermore, there is very little topographical variation in the area, so that such effects can be ignored in the modeling, Extensive ground-truth measurements were made in these areas, as will be discussed next.

2.2. Ground Truth

For each of the stands, nine circular plots, each with a 5m diameter were chosen for canopy structure measurements. These were located randomly within a 500m radius of the flux tower. These measurements were then used to obtain a statistical mean and deviation for parameters in each stand. The quantities measured were density of trees, dbh, tree height, an estimate of the number of primary branches.

percent canopy cover. To obtain a more accurate estimate of the average number of primary branches and to measure the number of secondary branches, needle density, and branch orientation angles, destructive measurements were performed. To do so, one "average" tree was cut in each stand, and the above quantities measured and used as representative values. The "average" tree was defined according to the average dhb and height values already measured nondestructively. The forest floor was not rigorously characterized, but in the forest model it was assumed to be a Bragg rough surface of rms height variation of about 1cm.

On the day of the SAR flight, dielectric measurements of trunks, branches, needles, and soil were performed using C- and L-band probes by another BOREAS investigation team (RSS-15). No measurements were obtained at P-band, Also on the day of the flight, we obtained gravimmetric soil moisture measurements for the 0-5cm layer using the can method, Ten samples were taken at each site.

A summary of the ground truth data for the YJP and OJP stands under study in this paper is presented in Table 1, It was assumed that the values of dielectric constant do not, change significantly across the frequency range between P-band and C-band, which is a valid assumption in lieu of the results published in [7,8] and the above-mentioned BOREAS field measurements.

3. OBSERVATIONS **FROM SAR DATA**

Figure 3 is a red-green-blue overlay of total power P-, L-, and C-band radar backscatters, respectively, obtained over the area mentioned in 2.1. above. The SAR image consists of 1280 lines and 1024 pixels per line. The OJP stand to be studied here is outlined with a solid line in the image, and the YJP with a broken line, Visual inspection reveals that over the OJP, magnitude of total power P-band return is much stronger than the other two bands, (shown in the image as bright orange) whereas for the YJP, the backscatter level in none of the three frequencies strongly dominates the others.

Tables 2(a) and 2(b) show some representative values from SAR data for HH, VV, and HV returns at C-, L-, and P-ands for YJP and OJP, respectively, The value of backscatter at each point shown in the tables (pixel-line pair) is found by averaging the corresponding values over a 5 x 5 box centered at that point. The aircraft flight parameters are_such that the center of YJP stand is at 42° incidence angle and that of the OJP at 52°. Some observations from these data are:

- The OJP HH return at P-band is 8-9 dB higher than that for YJP.
- The OJP HH return at P-band is about 5 dB higher than that at L-band and 79 dB higher than that at C-band.

- The HH return is about 8 dB higher than VV at P-band for the OJP
- .4t L- and C-bands, corresponding copolarized backscattering cross sections are similar in magnitude for OJP and YJP.
- At all frequencies, the magnitude of the HH return is larger than that of VV return for OJP. The same is true for YJP at C- and L-bands, but not at P-band.

The most distinct result is that the P-band HH return over the OJP stand is much higher than VV and that at the YJP. Comparison of the SAR image with the area's land cover map indicates that this result can be used to identify the OJP stands over the entire area with high level of accuracy, In the following sections, we will look at a forest scattering model and use ground truth measurement to identify the reason for this effect, as well as explain the other backscattering behaviors observed over these two forest types,

4. ANALYSIS OF SCATTERING MECHANISMS

4.1. Forest Scattering Model

Several discrete-component forest scattering models, e.g., those reported in [9] and [10], have been developed in the recent years. Here, we used a two-layer model developed at JPL by Durden et al. [9], in which tree trunks are modeled as a layer of nearly vertical cylinders, and the branches as a layer of randomly oriented cylinders. The orientation angle α with respect to the vertical for the branch layer cylinders has a probability density function given by $\sin^4\alpha$. This layer includes two different distributions, accounting for primary and secondary branches. The model also incorporates needles and leaves, as appropriate, in the branch layer. The model allows for the trunk layer to extend into the branch layer. The scattering from each layer is calculated using a first order (Born) approximation. The forest floor is modeled as a Bragg rough surface,

With the above components, the model includes contributions from 1) ground, 2) branch layer, 3) trunk-ground double bounce, 4) branch-ground double bounce. The wave attenuations through the branch and trunk layers are taken into account by averaging the elements of the forward scattering amplitude matrix over all cylinder orientations. _

4.2. **Classification**

Before proceeding to the analysis of scattering mechanisms using the forest model and ground truth data, it is instructive to use a classification algorithm, based only on simple scattering models and without any ground truth information, to obtain

an approximate indication of the scattering contributions involved at each location throughout the image.

A few unsupervised classification methods have been previously proposed, e.g., in [5] and [1 1]. We used the method of Freeman et al. [11], which considers contributions from single-bounce scattering from the ground, double-bounce scattering, and volume scattering, and derives their relative effects based on second order statistics of backscattered powers at various polarizations and frequencies, The result of application of such an algorithm is shown in Figure 4. Using the legend provided on the figure, this algorithm suggests that at C- and L-bands, volume scattering dominates at both YJP and OJP stands, whereas at P-band, the backscatter is mostly double-bounce at OJP, and a mix of double-bounce and volume at YJP. We will see in the next subsection that these results are generally in agreement with the results obtained from the forest scattering model using our ground-truth information.

4.3. **Discussion of Major Scattering Contributions**

Breakdown of Scattering Mechanisms

Given the ground truth measurements of Table 1, the above scattering model was used to calculate the contributions to the total backscatter from each mechanism. Table 3 shows the results for HH, VV, and HV polarizations for both the YJP and OJP, which are located at 42° and 52° incidence angles, respectively. The total backscatter is in good agreement (l-2 dB) with the actual SAR data for HH and VV, with the calculated HV return losing its accuracy with decreasing frequency.

It is observed that at C-band, at both YJP and OJP stands the radar backscatter is almost entirely due to branch-layer volume scattering at all polarizations. At this frequency, the incident field cannot penetrate into the canopy beyond the branch layer, and hence the radar measurement are not directly sensitive to quantities such as trunk heights and surface parameters. On the other hand, and for the same reason. the backscatter at C-band is highly dependent on the branch layer parameters such as primary and secondary branch diameter, length, dielectric constant, density, and orientation angle. However, notice that the level of radar backscatter at this single frequency is quite comparable for each polarizations for both stands given the measurement and calibration accuracy of SAR_1 and hence not enough information is provided to distinguish the two.

At L-band, the YJP backscatter remains mainly due to scattering from the branch layer, Trunk-ground scattering has a much smaller effect, as well as branch-ground and ground contributions. These are due to the very dense branch layer in the YJP area, which not only strongly backseat ters the incident waves, but also attenuates the transmitted wave, thus inhibiting subsequent backscatter from the layers beneath.

Furthermore, the effect of trunk-ground scattering is not significant, due to the roughness of forest floor at this frequency in addition to the small trunk size. On the other hand, the radar backscatter from the OJP stand is seen to be primarily due to trunk-ground double bounce scattering, with a small but still significant amount of branch layer contribution. This is because the longer wavelength at L-band can penetrate the OJP branch layer to a larger extent, due to its sparsity compared to that of the YJP. At the same time, the OJP trunks are about 4 times taller and have dbh values which are about 3 times larger, hence causing larger induced currents on the cylinders. The HH polarization is particularly higher than VV, since the vertically polarized incident waves are at an angle of 90-52=38 degrees with the tree trunks (true vertical direction), hence a smaller V-pol induced current, and also since the VV ground (rough surface) reflection coefficient is smaller than the HH case, The HV return, however, is still mostly caused by volume scattering from the branches,

As we move to P-band, the effect of branch layer backscatter decreases at both stands, with the trunks and ground (which is now smoother with respect to the wavelength) playing a more important role, since the branch layer with the smaller scatterers compared to the wavelength becomes more "transparent" to the incident waves. This effect is particularly obvious for the OJP, which has the more sparse branch layer. Furthermore, the large trunks of the OJP stand and the smooth ground cause strong double bounce scattering to be measured by the S. AR. The HH return is again higher in this case because of the incidence angle and ground reflection coefficient effects as discussed in the previous paragraph, The HV return for OJP does not agree very well with the SAR data since the present first-order scattering model does not accurately account for the cross-pol effects. For the YJP stand, branch-layer volume scattering is also no longer the dominant mechanism: the HH backscatter, which is less than VV, is mainly from the branch-ground double scat t ering mechanism with some contribution from branch layer volume scattering, and the VV backscattered fields are mostly due to the trunk-ground double bounce. The incidence angle effect is again observed here, except that in this case, it works in favor of the VV return, since the vertically polarized incident waves are now at 90-42=48 degrees with respect to the vertical cylinders, inducing larger currents on the dielectric cylinders as opposed to the case of OJP. Note that in the case of branch-ground scattering. tile HH component is much larger than VV since the primary and secondary branch orientation angles have a distribution with a peak value near the horizontal direct ion. so t hat stronger horizontally polarized fields are reradiated. This statement is in fact true at all frequencies for both the branch layer volume scattering and the branch-ground scattering,

Incidence Angle Effect

To better illustrate the effect of incidence angle on each scattering mechanism responsible for the total radar backscatter. we have used the forest scattering model with the canopy parameters of both YJP and OJP. Figures 5, 6, and 7 show the results

for C-, L-, and P-bands, respectively. Ground surface scattering is not shown in these figures, since it is generally much smaller than the other three mechanisms for these forests,

At C-band, it is seen that branch-layer contribution is dominant at all incidence angles examined, with trunk-ground and branch-ground backscatter cross sections at best 25 dB smaller. Nevertheless, for the OJP forest, the double-bounce mechanisms for both HH and VV polarizations show an increase of about 40 dB over the 25-60 degree incidence angle range, whereas their range of variation for the YJP forest is about 10 dB.

The total radar backscatter at L-band contains the effects of the two double-bounce mechanisms to a larger extent than at C-band. In particular, in the OJP forest both polarizations include a significant contribution from trunk-ground scattering as well as that from the branch layer for all incidence angles. For YJP, although trunk-ground scattering is more pronounced than that at C-band, it is still subdominant to the branch-layer scattering, and decreases with increasing incidence angle. Branch layer contribution also decreases for both forests as the incidence angle increases, partly due to wave attenuation in the canopy.

The Trunk-ground double-bounce scattering becomes the main contributor at P-band in the OJP forest for all incidence angles, with branch layer volume scattering and branch-ground double-bounce distant contenders. The VV backscatter has a larger magnitude than HH for incidence angles up to about 47 degrees, after which it becomes smaller, due to the tradeoffs between the component of the current induced on the trunks by the incident field and reflection coefficient of the rough surface representing the forest floor. For the HH backscatter in the young Jack Pine forest, the branch layer still plays an important role both in single - bounce (volume) and double-bounce capacities. For VV polarization, trunk-ground double-bounce scattering contributes the most to the total backscatter cross section at all incidence angles, although at smaller angles, the branch layer is also significant.

The above results, both from measured S.4 R data and from model simulation>. suggest that the mere knowledge of total backscatter amplitude is not sufficient to uniquely characterize a forest and identify its components as they contribute to radar measurements, and neither are SAR measurements at a single frequency and/or polarization. Rather, it is the polarimetric information of each of the major scattering mechanisms at various frequencies that might lead to a distinct characterization of forest canopy components. As we saw earlier in this section, at each frequency and for each polarization, a different scattering mechanism may dominate depending on the forest type and incidence angle. We are currently utilizing the information thus provialed in developing quantitative inversion algorithms which retrieve various canopy

parameters based on the breakdown of the total radar backscatter into individual mechanisms.

5. CONCLUDING REMARKS

The AIRSAR measurement of young and old Jack Pine stands in the Canadian boreal forest demonstrated distinct signatures for polarimetric SAR data at C-, L-, and P-bands, The observations were analyzed and discussed using a forest scattering model which incorporates the effects of four major scattering mechanisms. It was shown that for each forest type and at each incidence angle, the magnitude of the polarimetric total backscattered signal was not necessarily a unique and descriptive measurement, but rather it was the contributions from various scattering mechanisms that provided more insight into the specific physical scattering process. The observation that in each case a different set of scattering mechanisms is responsible for the total backscattered signal is a consequence of the different forests having different branch and trunk layer architectures, different floor characteristics, and different component dielectric constants. Such information, along with unsupervised classification algorithms, is being used in developing inversion algorithms for retrieving forest canopy parameters depending on the relative contribution of these scattering mechanisms, e.g., as in [12]. The current study hence serves as a motivation and explanation for the ongoing work on the development of our mechanism-based inversion technique.

ACKNOWLEDGEMENT

The work described here was performed by the Jet Propulsion Laboratory, California Institute of Technology, under a contract from the National Aeronautics and Space Administration. The authors wish to thank A. Freeman for allowing the use of the three-component classification algorithm and S. Durden for providing them with the forest scattering program.

REFERENCES

[1] T. Le Toan, A, Beaudoin, J. Riom, and D.Guyon, "Relating forest biomass to SAR data," *IEEE Trans.Geosci.Remote* Sensing, vol. 30, pp. 403-411,1992.

[2] M. C. Dobson et al., "Dependence of radar backscatter on conifer forest biomass, " *IEEE Trans.Geosci. Remote Sensing*, vol. 30, pp. 412-415, 1992.

[3] K. J. Ranson and Q. Sun; "Mapping Biomass of a Northern Forest Using Multifrequency SAR Data," *IEEE Trans. Geosci.Remote Sensing,* vol. 32, pp. 388-396, March 1994,

[4] M. Moghaddam, S. Durden, and H. Zebker, "Radar Measurement of Forested Areas During OTTER," *Remote Sensing Environ.*, vol. 47, pp. 154-166, Feb. 1994.

[5] J. J. van Zyl, "Unsupervised classification of scattering behavior using radar polarimetry data," *IEEE Trans.Geosci. Remote Sensing*, vol. 27, pp. 36-45, 1989.

[6] BOREAS Experiment Plan, Chapter 1, Version 3.0, May 1994.

[7] W. A. Salas, K. J. Ranson, B.N. Rock, and K. T. Smith, "Temporal and spatial variations in dielectric constant and water status of dominant forest species from New England," *Remote Sensing Environ.*, vol. 47, pp. 109-119, Feb. 1994.

[8] M. A. El-Rayes and F. T. Ulaby, "Microwave dielectric spectrum of vegetation - Part I: Experimental observations," *IEEE Trans. Geosci. Remote Sensing,* vol. GE-25. no, 5, pp. 541-549, 1987.

[9] S. L. Durden, J. J. van Zyl, and H. A. Zebker, "Modeling and Observation of the Radar Polarization Signature of Forested Areas," *IEEE Trans.Geosci. Remote Sensing,* vol. *27,* pp. 290-301, 1989.

[10] R. H. Lang and J. S. Sidhu, "Electromagnetic backscattering from a layer of vegetation: A discrete approach ," *IEEE Trans.Geosci. Remote Sensing,* vol. 21, pp. 62-71, 1983.

[11] A. Freeman, S. L. Durden, and R. Zimmerman, "Mapping Subtropical Vegetation Using Multifrequency, Multipolarization SAR Data," *Proc.IGARSS'92*, Houston, TX, pp. 1986-1689, 1992.

[12] M. Moghaddam and S.Saatchi, "An Inversion Algorithm Applied to SAR Data to Retrieve Surface Parameters," *Proc.IGARSS '99,* Tokyo, Japan, August 1993.

Table 1. Forest parameters from ground-truth measurements used in backscatter modeling.

	YJP	OJP
tree density ($\#/m^2$)	1.0	0.3
canopy thickness (m)	2.8	9.0
trunk height(m)	3.8	15
trunk dielectric constant	(39,2)	(39,6)
dbh (cm)	4.0	13.0
primary branch density ($\#/m^3$)	30	7
primary branch dielectric constant	(39,2)	(39,6)
primary branch orientation (degrees)	80	80
primary branch length (m)	0.8	0.7
primary branch diameter (cm)	1.0	1.0
secondary branch density ($\#/m^3$)	300	70
secondary branch dielectric constant	(39,2)	(39,6)
secondary branch diameter (cm)	0.4	0.4
soil dielectric constant	(8,1)	(7,1)

Table 2(a). Representative magnitudes in dB for HH, VV, and HV SAR data from young Jack Pine stand in the boreal forest.

stand(pixel,line)	P-HH	P-VV	P-HV	L-HH	L-VV	L-HV	C-HH	C-VV	C-HV
YJP(319,350)	-9	-7	-18	-6	-8	-14	-9	-11	-15
YJP(343,336)	-8	-6	-19	-6	-8	-14	-9	-12	-15
YJP(351,321)	-9	-6	-19	-5	-7	-13	-8	-lo	-13
YJP(305,329)	-9	-7	-18	-6	-7	-14	-8	-9	-14
average	-8.8	-6.5	-18.5	-5.8	-7.5	-13.8	-8.5	-10.5	-14.3

Table 2(b). Representative magnitudes in dB for HH, VV, and HV SAR data from old Jack Pine stand in the boreal forest.

stand(pixel,line)	P-HH	P-VV	P-HV	L-HH	L-VV	L-HV	C-HH	C-VV	C-HV
OJP(557,576)	0	-8	-13	-5	-8	-lo	-7	-8	-13
OJP(525,634)	0	-8	-14	-5	-8	-12	-8	-10	-14
OJP(522,558)	0	-7	-14	-5	-8	-8	-9	-8	-15
OJP(638,646)	-1	-9	-13	-5	-8	-lo	-7	-6	-13
average	-0.3	-8.0	-13.5	-5.0	-8.0	-10.0	-8.0	-8.0	-13.8

Table 3(a). Model predictions, in dB, at P-band (wavelength =68 cm) given the parameters in Table 1.

	YJP, HH	YJP, VV	YJP, HV	OJP, HH	OJP, VV	OJP, HV
branch layer	-15	-17	-21	-22	-26	-'29
branch-ground	-14	-36	-39	-23	-44	-44
trunk-ground	-25	-9	-39	-2	-6	-24
ground	-34	-28		-34	-28	·
total	-11.4	-8.0	-'21.1	-1,5	-5.9	-22.4

Table 3(b). Model predictions, in dB, at L-band (wavelength =24 cm) given the parameters in Table 1.

	YJP, HH	YJP, VV	YJP, HV	OJP, HH	OJP, VV	OJP, HV
branch layer	-9	-9	-14	-lo	-12	-16
branch-ground	-27	-38	-48	-19	-34	-37
trunk-ground	-45	-47	-55	-6	-lo	-42
ground	-54	-44		-39	-29	-
total	-8.8	-9.4	-13.9	-4,3	-8.2	-15.7

Table 3(c). Model predictions, in dB, at C-band (wavelength= 5.6 cm) given the parameters in Table 1.

	YJP, HH	YJP, VV	YJP, HV	OJP, HH	OJP, VV	OJP, HV
branch layer	-9	-lo	-15	-lo	-11	-16
branch-ground	-36	-44	-57	-55	-64	70
trunk-ground	-33	-34	-68	-35	-40	79
ground	-42	-32		-35	-24	
tot al	-9,3	-10.2	-15.1	-10.3	-10.6	15 9

Figure Captions

Figure 1. Map of BOREAS Southern study area (SSA), with the .41RSAR flight lines superimposed. The flight line used in this work is shown with an asterisk.

Figure 2. Photographs of typical locations in the YJP and OJP stands.

Figure 3. RGB image of the P-L-C total power AIRSAR data over BOREAS' Prince Albert area.

Figure 4. Three-component classification of the polarimetric 3-frequency AIRSAR image.

Figure 5. Incidence angle dependence of C-band radar backscatter. (a) Total backscatter, (b) branch-layer contribution, (c) branch-ground double-bounce, (d) trunk-ground double-bounce,

Figure 6. Incidence angle dependence of L-band radar backscatter. (a) Total backscatter, (b) branch-layer contribution, (c) branch-ground double-bounce, (d) trunk-ground double-bounce,

Figure 7. Incidence angle dependence of P-band radar backscatter. (a) Total backscatter, (b) branch-layer contribution, (c) branch-ground double-bounce, (d) trunk-ground double-bounce.

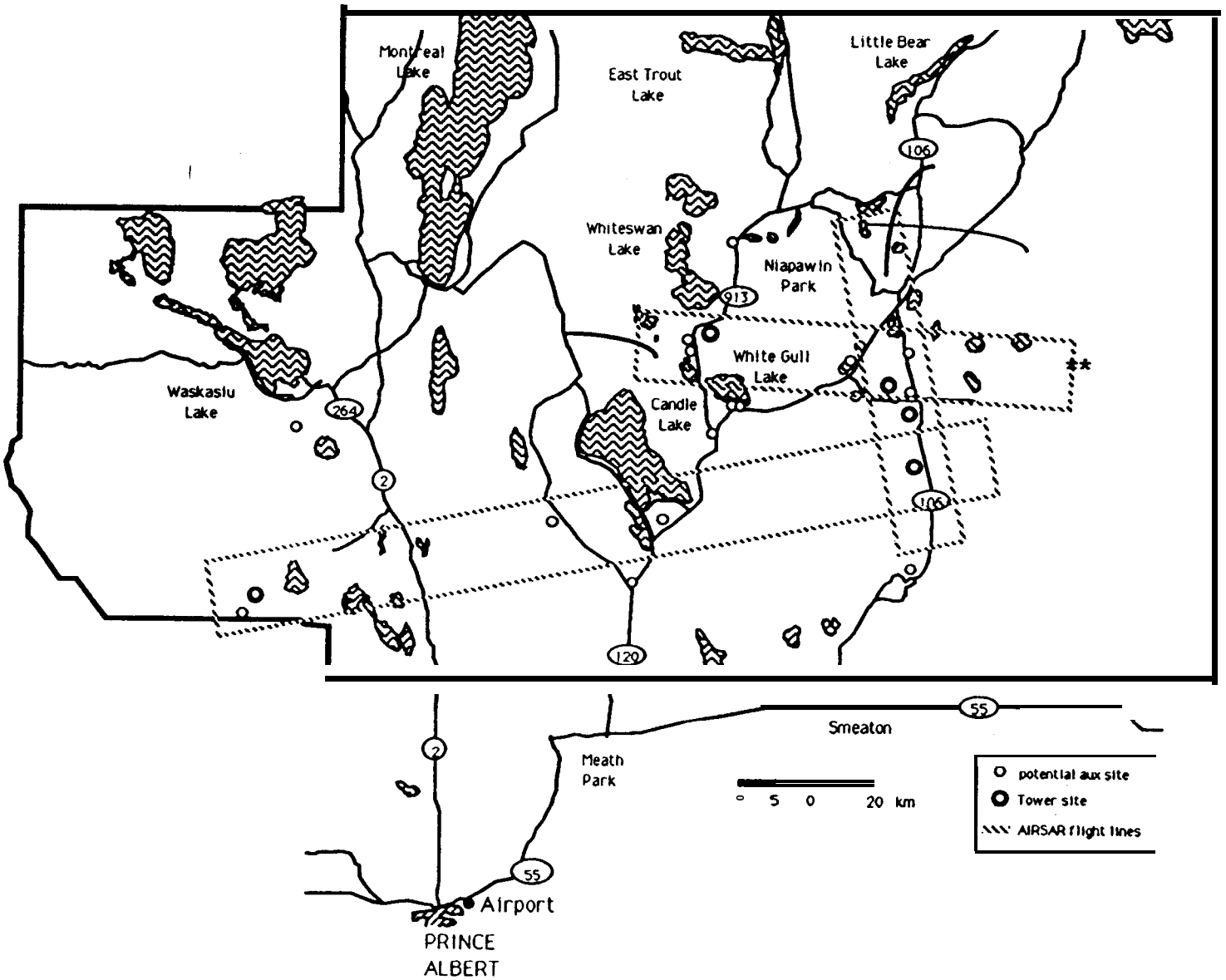
Montreal Lake
East Trout Lake
Little Bear Lake
106
Whiteswan Lake
Niapawin Park
913
White Gull Lake
Waskasiu Lake
264
Candle Lake
2
106
120
55
Smeaton
2
Meath Park
0 5 0 20 km
potential aux site
Tower site
AIRSAR flight lines
55
Airport
PRINCE ALBERT

Figure 1

YOUNG JACK PINE

OLD JACK PINE

Figure

Figure 2

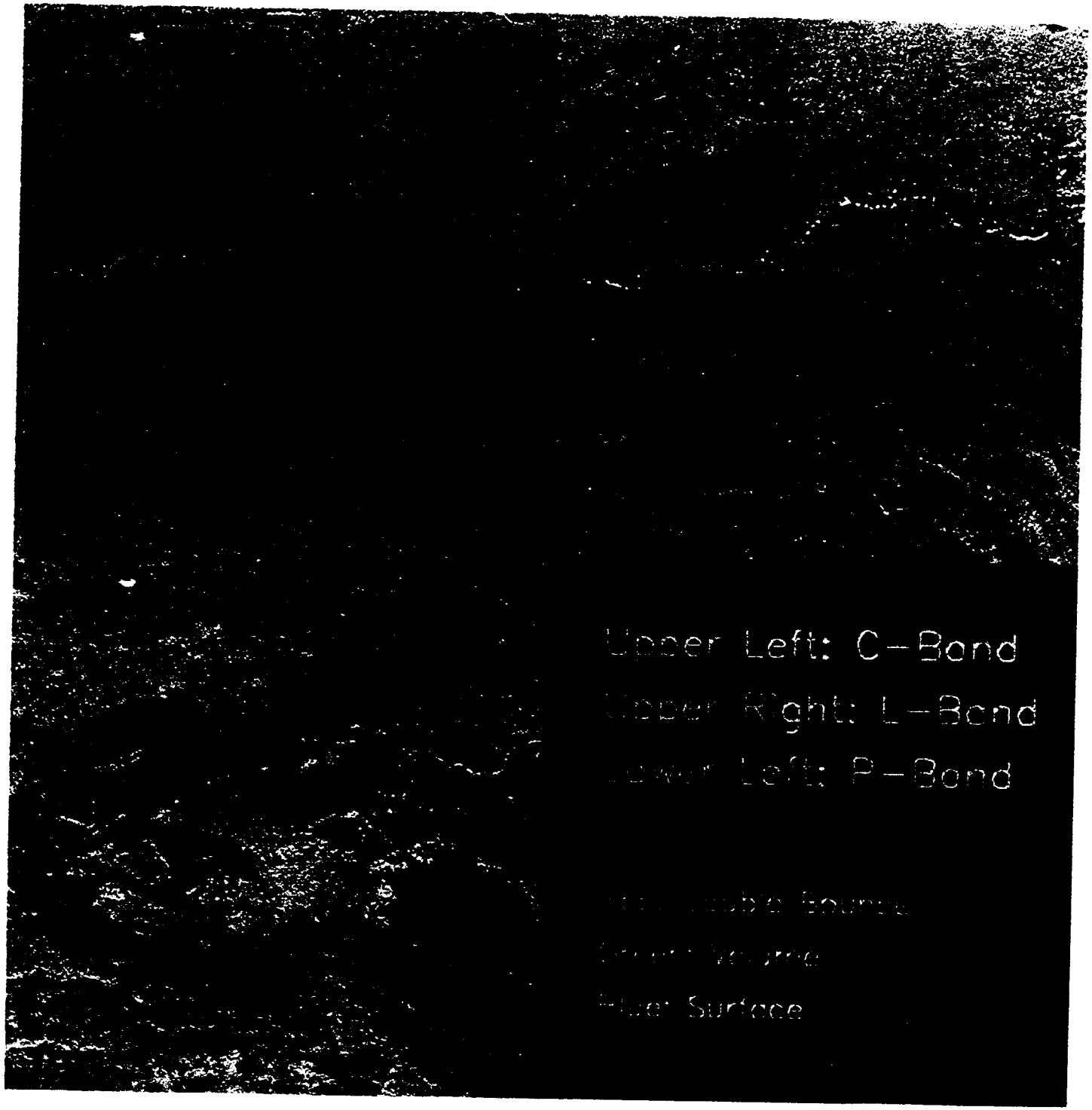

Figure 4

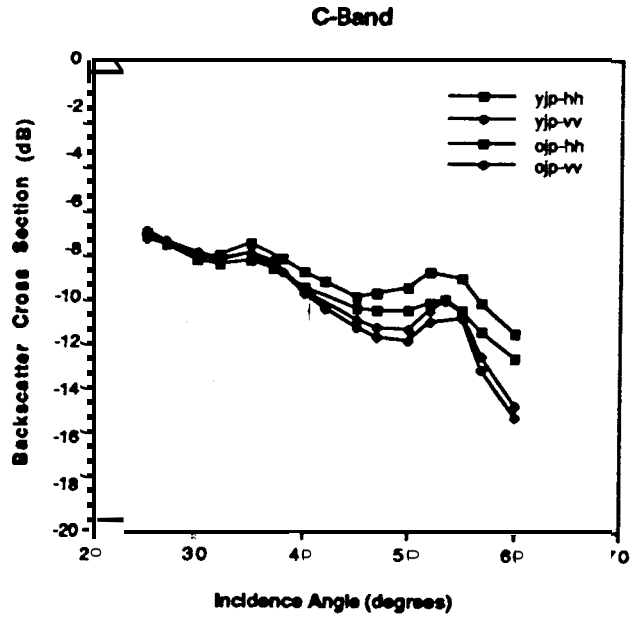
C-Band
yjp-hh
yjp-vv
ojp-hh
ojp-vv
Backscatter Cross Section (dB)
Incidence Angle (degrees)

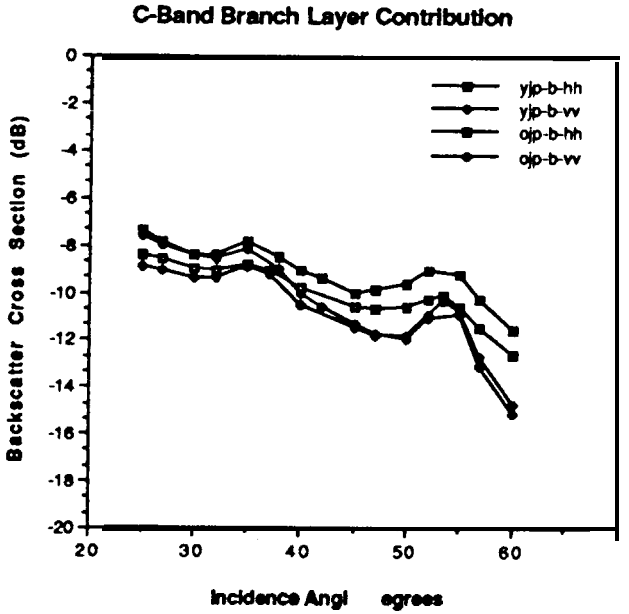
C-Band Branch Layer Contribution
yjp-b-hh
yjp-b-vv
ojp-b-hh
ojp-b-vv
Backscatter Cross Section (dB)
Incidence Angle degrees

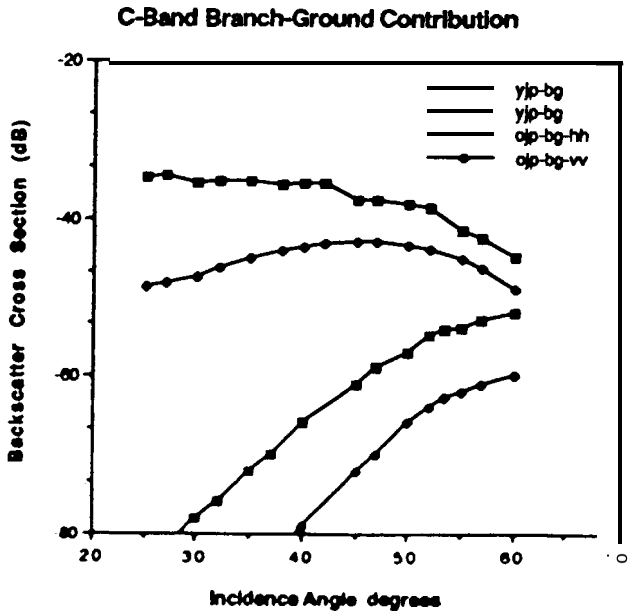
C-Band Branch-Ground Contribution
yjp-bg
yjp-bg
ojp-bg-hh
ojp-bg-vv
Backscatter Cross Section (dB)
Incidence Angle degrees

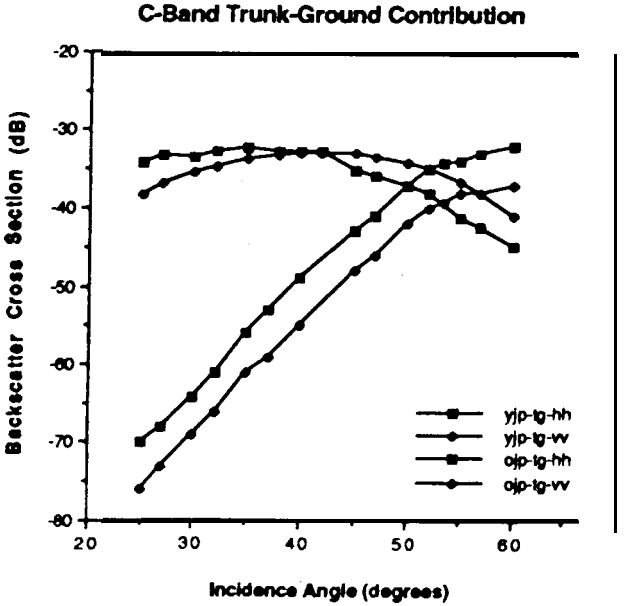
C-Band Trunk-Ground Contribution
yjp-tg-hh
yjp-tg-vv
ojp-tg-hh
ojp-tg-vv
Backscatter Cross Section (dB)
Incidence Angle (degrees)

Figure 5

L-Band

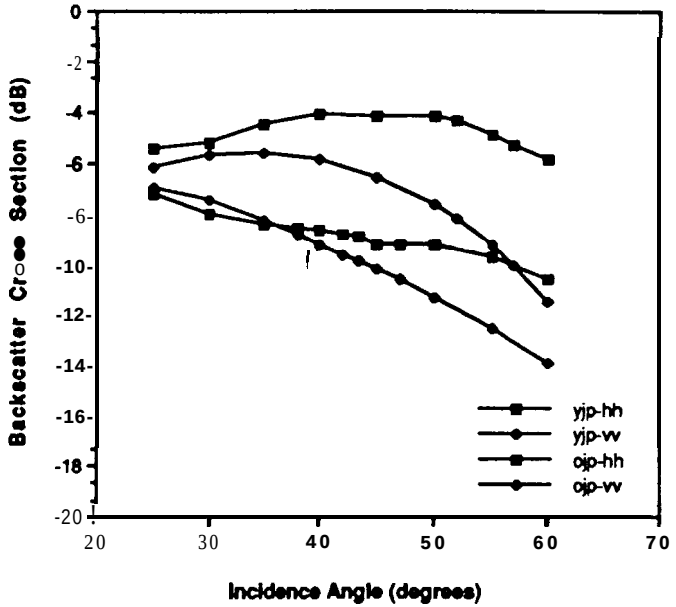

L-Band Branch Layer Contribution

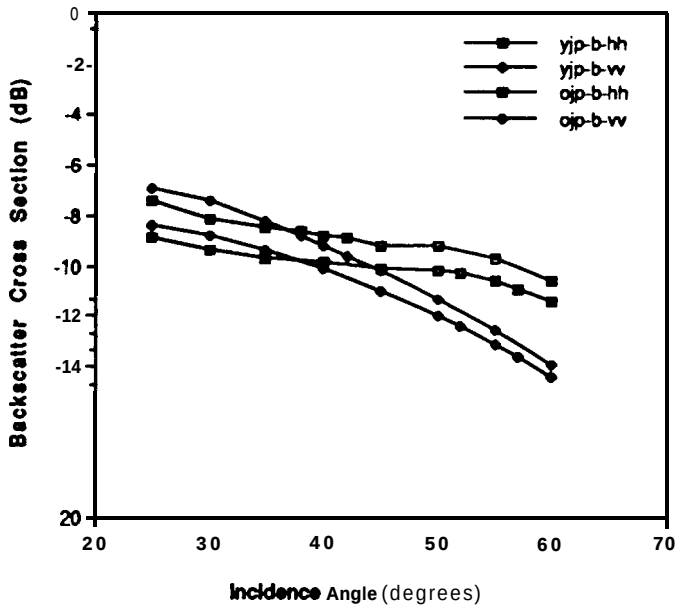

L-Band **Branch-Ground Contribution**

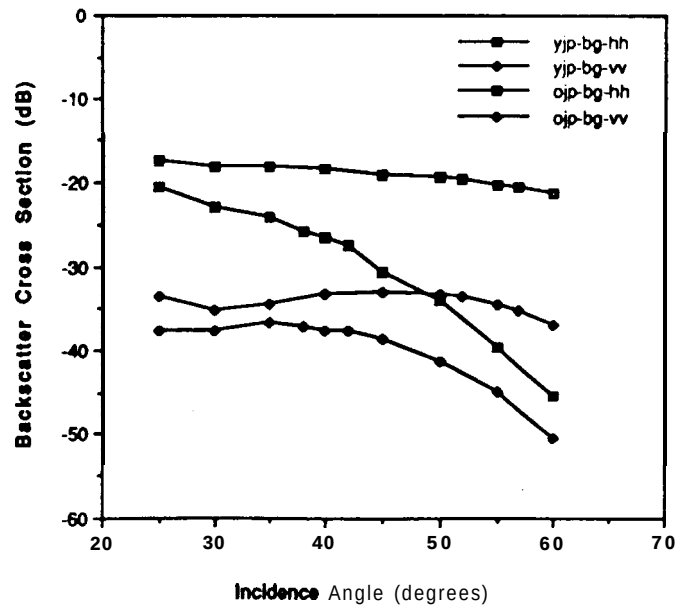

L-Band **Trunk-Ground** Contribution

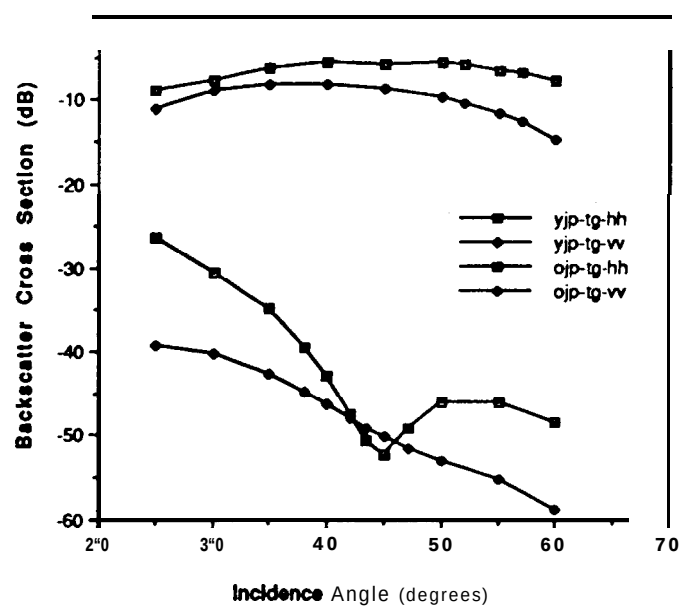

Figure 6

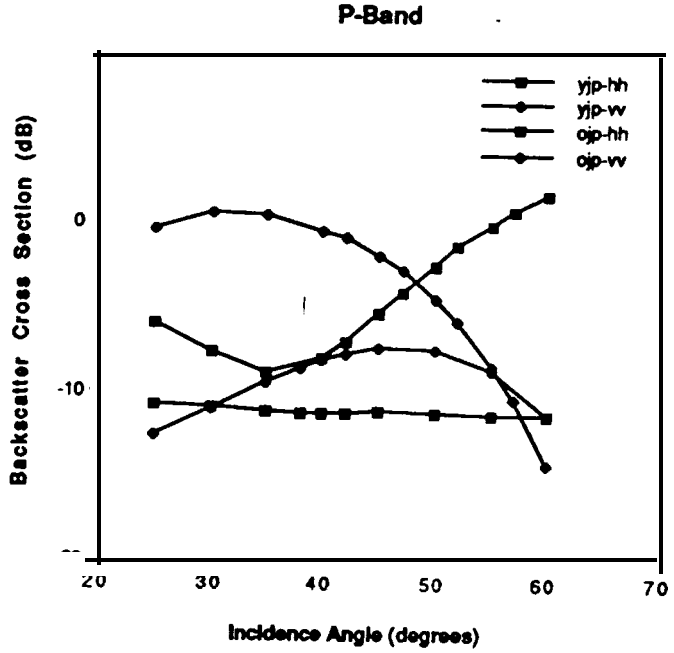
P-Band
yjp-hh
yjp-vv
ojp-hh
ojp-vv
Backscatter Cross Section (dB)
0
-10
20
30
40
50
60
70
Incidence Angle (degrees)

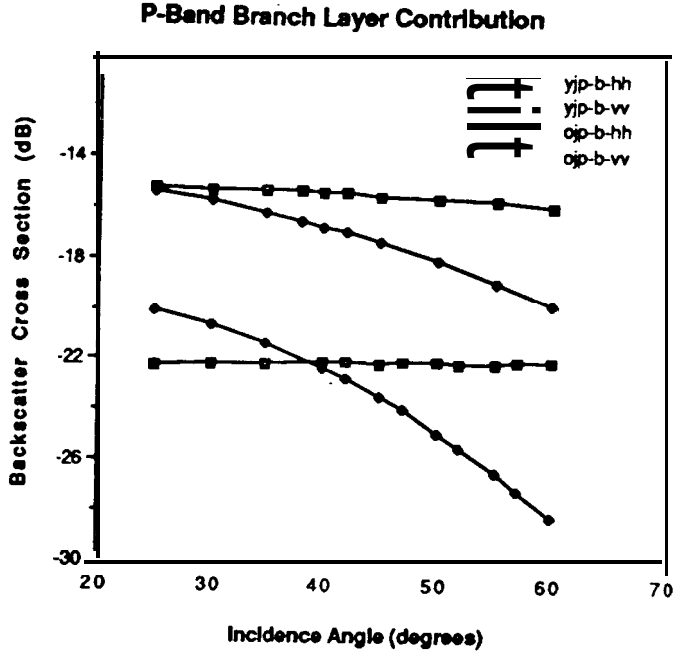
P-Band Branch Layer Contribution
yjp-b-hh
yjp-b-vv
ojp-b-hh
ojp-b-vv
Backscatter Cross Section (dB)
-14
-18
-22
-26
-30
20
30
40
50
60
70
Incidence Angle (degrees)

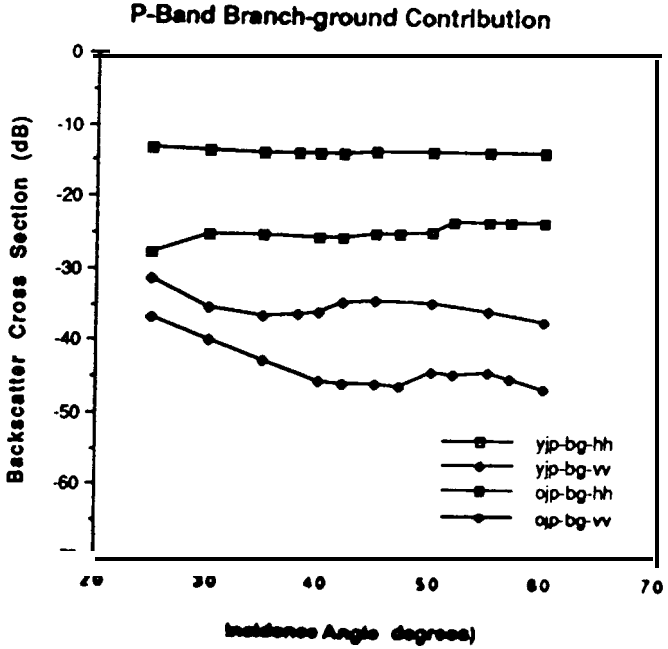
P-Band Branch-ground Contribution
yjp-bg-hh
yjp-bg-vv
ojp-bg-hh
ojp-bg-vv
Backscatter Cross Section (dB)
0
-10
-20
-30
-40
-50
-60
70
Incidence Angle degrees)

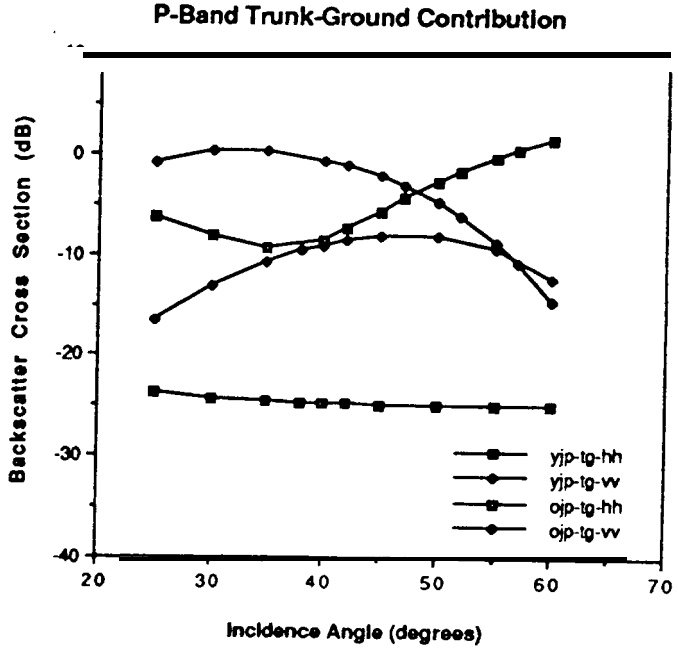
P-Band Trunk-Ground Contribution
yjp-tg-hh
yjp-tg-vv
ojp-tg-hh
ojp-tg-vv
Backscatter Cross Section (dB)
0
-10
-20
-30
-40
20
30
40
50
60
70
Incidence Angle (degrees)

Figure 7